Chapter@3

Effect of graphene on polyurethane properties

3.1 Introduction:

Polyurethanes (PUs) represent a class of polymeric material which is widely used in medical, automotive and industrial fields due to its unique properties [Howard et al. (2002)]. Polyurethane has been synthesized using polyol, diisocyanate and chain extender [Ciardelli et al. (2004)]. Properties of PUs can be easily modified either by changing the composition or by changing the chemistry of polyol, diisocyanate and chain extender or by using the suitable filler in polymer matrix [Mishra et al. (2010)]. The Segmented nature of PU arises from its hard and soft zone and depending upon these segmental composition and specific interactions between them (hard-hard, hard-soft and soft-soft region) varying shapes like cylindrical or lamellar, globular and fibrillar structures are formed originating from the interconnected hard/soft domain network [Mishra et al. (2010)]. Now a day, self-assembled PUs have drawn the wide attention and extensively used in tissue engineering, shape memory materials, molecular recognition and drug delivery applications and the nature of these polymeric self-assemblies can be altered by changing the chemical structure and constituents of polymer or by using fillers in the matrix [Peppas et al. (1999); Lendlein et al. (2005); Mishra et al. (2012)]. Various types of fillers are being used to improve polymer properties and these improvements in properties depend upon the shape, size, aspect ratio and surface modification of the fillers [Zilg et al. (1999)]. Due to the high shape recoverability, good processing ability, low cost as well as wide temperature range for recovery PU have a wide range of applications in medical sciences as smart actuators and in aerospace and textile engineering [Lendlein et al. (2002); Gordon et al. (1994)].

Recently, different modified layered silicates as well as carbon in different forms like carbon black, carbon nanotubes (CNTs) are extensively used in synthesis of polymer nanocomposites [Moniruzzaman et al. (2006); Li et al. (2000)]. Carbon has different allotropic structure like 0-D (fullerenes), 1-D CNTs and nanoribbons, and 2-D graphene sheet structure. Fullerene can be made by wrapping a section of graphene sheet whereas CNTs and nanoribbons by rolling and slicing of graphene sheet [Kim et al. (2010)]. Improvement in shape memory and mechanical properties of hyperbranched PU has been reported through dispersion of CNTs in matrix [Kuan et al.(2005); Cho et al. (2005)]. Whereas, round shaped polyhedral oligomeric silsesquioxane (POSS) attached to thermoplastic PU suppresses the enzymatic degradation of PU by preventing the ester linkages from enzymatic attack [Gu et al. (2011)].

Graphene is a single layered of carbon atom with sp^2 hybridized and hexagonally arranged structure [Geim et al. (2007)]. Graphene have a number of extraordinary optical, electrical, thermal and mechanical properties [Novoselov et al. (2004); Lalit et al. (2006)]. Due to its high surface area (2630 m^2/g), with superior electronic conductivity i.e. (electron mobility ~ 2×10^5 cm^2 V/s), mechanical strength (Young's modulus ~1100 GPa) and biocompatibility of graphene sheet, it has potential to be used as filler for polymeric matrices [Shen et al. (2012)]. Recently graphene oxides or surface functionalized graphene have been used as nanofiller for PU to unprove the mechanical, thermal [Wang et al. (2011)], gas barrier, electrical conductivity [Kim et al. (2010)], and shape memory effect [Choi et al. (2012)] using predominantly aromatic based PUs have been reported in the literature. Pure graphene sheets exhibit the

biocompatible nature using bone marrow derived mesenchymal stem cells (BMMSCs) and have the potential to be used in tissue regeneration [Lee et al. (2011)] but it is required to have support like polymer for its use as potential implant. To the best of our knowledge, there is no literature report is available about graphene induced self-assembly in PU and the effect of the self-assembly on practical applications such as controlled drug delivery and its potential use as biomaterials.

This chapter deals the effect of embedding two-dimensional graphene sheet in PU matrix and to explore the layer by layer self-assembly (nanoscale to microscale) in PU in presence of graphene. Incorporation of graphene filler in early stage of in-situ polymerization process is responsible for uniform dispersion of graphene in polymer matrix. Numerical value in nanocomposites indicates the weight% of graphene in polyurethane matrix.The effect of self-assembly on mechanical, thermal and rheological properties has been studied in detail both in solid and liquid state showing structure property relationship of supramolecular PU. Small-angle neutron scattering (SANS) and X-ray diffraction (XRD) technique is used for evaluation the structure of nanocomposites. Surface morphology of pure PU and its different nanocomposites was studies through atomic force microscope (AFM) and optical microscope (OM). The thermal behavior of PU and its nanocomposites is revealed through thermo gravimetric analyzer (TGA) and differential scanning calorimeter (DSC). Degradation response of pure polyurethane and its nanocomposites was monitor with *lipase* and *protease* enzyme. Control release of tetracycline loaded drug has been demonstrated by regulating the size of assembly in presence of graphene.

3.2 Results and discussion:

3.2.1 Dispersion and self-assembly:

Properties of materials are highly influence by the dispersion nature of filler into polymer matrix. In-situ polymerization technique in which graphene sheet is incorporated at early step of polymerization leads the uniform dispersion of graphene in PU matrix is evident from the bright filed TEM image. Due to this uniform dispersion individual graphene layer is wrapped up with growing polymer chain. Graphene layers have weak van der Waals interactions which facilitate the homogeneous dispersion into individual sheets in small molecular organic media [Cao et al. (2011)]. Here polymerization occurs in between the gallery leading to almost individual graphene layer encapsulated with PU chains. In-situ polymerization cause very good dispersion of individual graphene of lateral dimension of ~15 nm and expected to improve the overall properties of the composites in presence of graphene (Figure 3.1).

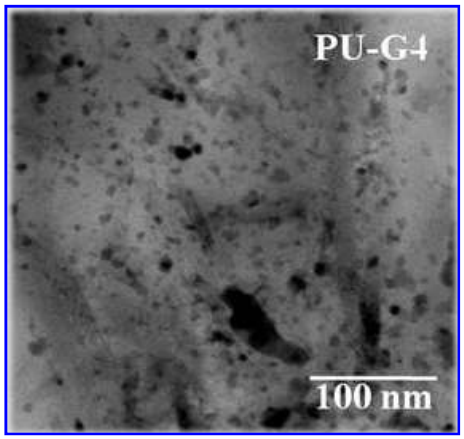

Figure 3.1: Bright field transmission micrograph of indicated PU nanocomposite (4wt% graphene)

Agglomerated morphology is observed when graphene is incorporated at the last step of polymerization i.e. in polymer solution. This is due to the high viscous nature of polymer solution restrict the dispersion of the individual graphene sheet. TEM image of polyurethane / graphene nanocomposites form at the last step of polymerization is given in (Figure 3.2).

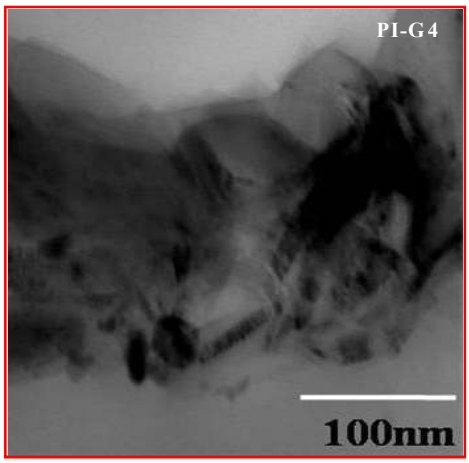

Figure 3.2: Bright field transmission electron micrographs of nanocomposites (4 wt% graphene) in polymer soloution, showing the stacking nature of graphene in polymer matrix.

Pure PU shows a X-ray diffraction peak at 2q ~7.2^0 with corresponding d-spacing of 1.2 nm (Figure 3.3a) which has been shifted towards higher angle on addition of graphene indicating lower interplanar distances in composites (1.08 nm). In pure PU this diffraction peak is arise due to the formation of molecular sheet through strong hydrogen bonding interaction between urethane linkages while this distance becomes shorter in hybrids possibly due to strong interaction between PU chains and graphene. Domain structure in pure PU and its nanocomposites was observed through small angle

neutron scattering (SANS) in the q range of 0.17-3.5 nm^{-1}. Appearance of a peak in pure PU at q ~0.4 nm^{-1}, with corresponding characteristic length ($\Lambda_c = 2\pi/q_m$)) of ~16 nm, indicates another nanostructure (Figure 3.3b) while the peak has been shifted to higher q at Λ_c = 10 nm for PU-G2, indicating close packing in PU nanocomposites. This decrease in the characteristic length in nanocomposites (~10 nm) as compared the pure PU (~16 nm) indicates the much closed packaging is occurred and lesser number of molecular sheets required forming an assembly in presence of graphene layers. At higher content of graphene no such peak is observed due to the limitation of our instrument and as well as larger agglomeration in presence of greater amount of fillers. The SANS patterns are best fitted in Debye-Bueche model (eq.1) especially in the lower q range to calculate the correlation length (ξ) and has been plotted in the inset figure of (Figure 3.3b). The calculated values of correlation length are 0.8, 2.64, 2.80, 2.82 and 2.94 nm for PU, PU-G2, PU-G4, PU-G6 and PU-G8, respectively, indicating higher correlation length (ξ) for composites.

$$I(q) = I(o) / (1+ \xi^2 q^2)^2 \qquad (1)$$

Where, I (q) is the scattered intensity, and q is the wavevector, ξ is the correlation length and I (o) is the extrapolated structure factor at zero wavevector.

There is various applications of π-stacked molecular sheet preferentially π-conjugated polymer system [Prosa et al. (2011)] however, this is the first time to report the formation of molecular sheet structure in polyurethane in presence of graphene. Surface morphology of pure PU and its nanocomposites are studies through AFM and optical microscope. AFM topographs in tapping mode have been presented in (Figure

3.3c) comparing the surface morphology of pure PU and nanocomposites showing compact crystallites in nanocomposites arising from the hard segment assembly as compared to pure PU which is further cleared from the relatively higher intensity of height profile and smaller in dimension in nanocomposites as compared to pure PU. Moreover, the size of the crystallites is in the range of ~0.5 mm as observed through AFM topographs. The optical images under cross-nicol microscope clearly exhibit the inhomogeneities of dimension around 5 mm of primarily the larger crystallites of polymer whose size gradually decrease in nanocompositess and more specifically the size decreases with increasing the graphene content in the hybrids (Figure 3.3d). This is first report of forming molecular stacks in PU in presence of graphene layers. Interestingly, the formation of nanostructure and self-assembly is evident from the gradual increase of interplanar spacing of 1.2 nm in X-ray diffraction to 16 nm Bragg's reflection in SANS which eventually form a larger cluster of size 500 nm as observed through AFM and subsequently construct a large crystallite of dimension 5 μm as witnessed in optical images. The reason for forming molecular sheets in PU is due to extensive intermolecular hydrogen bonding especially in hard segment zone and the molecular sheets are further associated through hydrogen bond making a larger cluster and ultimately big crystallites as observed through AFM and optical images, respectively. On contrary, the strongly correlated system of graphene composite is explained from the polar interactions between electron cloud on and over the graphene sheet and dipole of urethane linkages and, thereby, predicts the shorter interplanar distances in composites as compared to pure PU (Figure 3.3e). Stacking patterns from nanoscale to microscale assembly have been established in PU, which further

aggravated in presence of graphene in nanocomposites predominantly through secondary forces of hydrogen bonding and dipolar interactions.

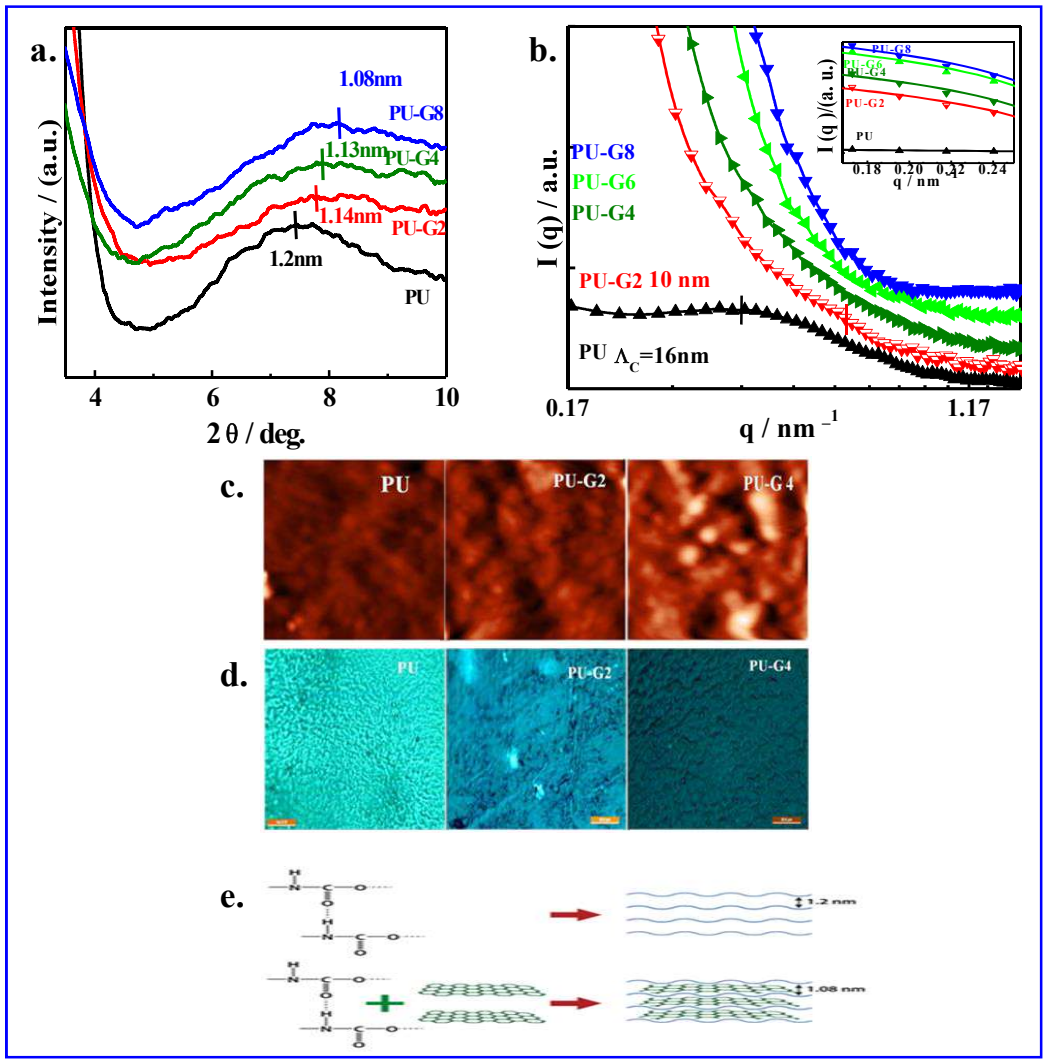

Figure 3.3 (a) X-ray diffraction patterns of PU and its indicated nanocomposites. Vertical lines indicate the peak position with interplanar spacing; **(b)** Small angle neutron scattering patterns; I (q) vs q (wave vector) plot of PU and its indicated nanocomposites. Inset figure shows the Debye-Bueche fitting for the calculation of correlation length, (ξ); **(c)** AFM images of PU and its indicated nanocompositess (5μm × 5μm) obtained through tapping mode **(d)** Polarizing optical images of PU and its indicated nanocomposites; **(e)** Schematic representation of stacking showing the interaction site without and with graphene layers in pristine PU and nanocomposites.

3.2.2 Interaction:

Interaction between urethane linkage and graphene which is responsible for self-assembled structure in pure PU and its nanocomposites is verified through the FTIR and UV-visible spectra and FTIR spectra is given in (Figure 3.4a,a') Absorption peak at 3320 cm^{-1} in PU and its nanocomposites is due to hydrogen bonded N-H stretching frequency in urethane moieties while the peak exhibit another hump towards higher frequency for lower graphene content composite which eventually gets prominent at 3354 cm^{-1} for higher graphene containing nanocomposites (PU-G8), clearly indicating the hydrogen bonded free N-H stretching frequency in nanocomposites [Raghu et al. (2008)]. Similar observation is also found in >C=O (carbonyl) stretching frequency at 1681 cm^{-1} peak for pure PU against new peak at higher frequency (at 1716 cm^{-1}) for higher graphene content nanocomposite. Significant suppression in intensity of hydrogen bonding in composites prepared through in-situ polymerization was also reported by Kim et al. [Kim et al. (2010)]. Intensity of the hydrogen bonded N-H and >C=O stretching peak gradually decrease with increasing graphene content in nanocomposites showing lesser hydrogen bonded interaction in nanocomposites. Hence, FTIR studies confirm the hydrogen bonded interaction is the major phenomenon in pure PU while hydrogen bonded free N-H stretching is prominent in nanocomposites. Interactions between polymer chains and graphene filler is also verified through UV-vis studies and given in (Figure 3.4b). Pure graphene exhibits an absorption peak at 230 nm has been shifted gradually to higher wavelength for higher graphene content composites confirming the good interaction between PU and graphene.

Melting behavior of Pure PU and its nanocomposites was studies through DSC thermogram and it was observed that pure PU shows double melting peaks at 24^0C, due to polyol (soft segment zone) melting, and at 168^0C arising from the hard segmented zone. The consistent depression of melting point is observed with greater graphene content in nanocomposites both for soft segment and hard segmented zone (Figure 3.4c). It is noteworthy to mention that depression of melting point occurs in case of interactive systems for the mixture of two components. The depression of melting point of hard segmented zone only is reported previously with nanoclay [Mishra et al. (2010)] while the interaction between graphene and PU takes place both through hard as well as soft segment making it a strongly interactive system throughout the whole polymer chain and graphene layers. Moreover, systematically decrease in the heat of fusion ΔH was obtained with increasing graphene content in nanocomposites both for soft and hard segment melting. The decreasing tendency of ΔH and T_m has been shown in (Figure 3.4d) as a function of graphene content in nanocomposites.

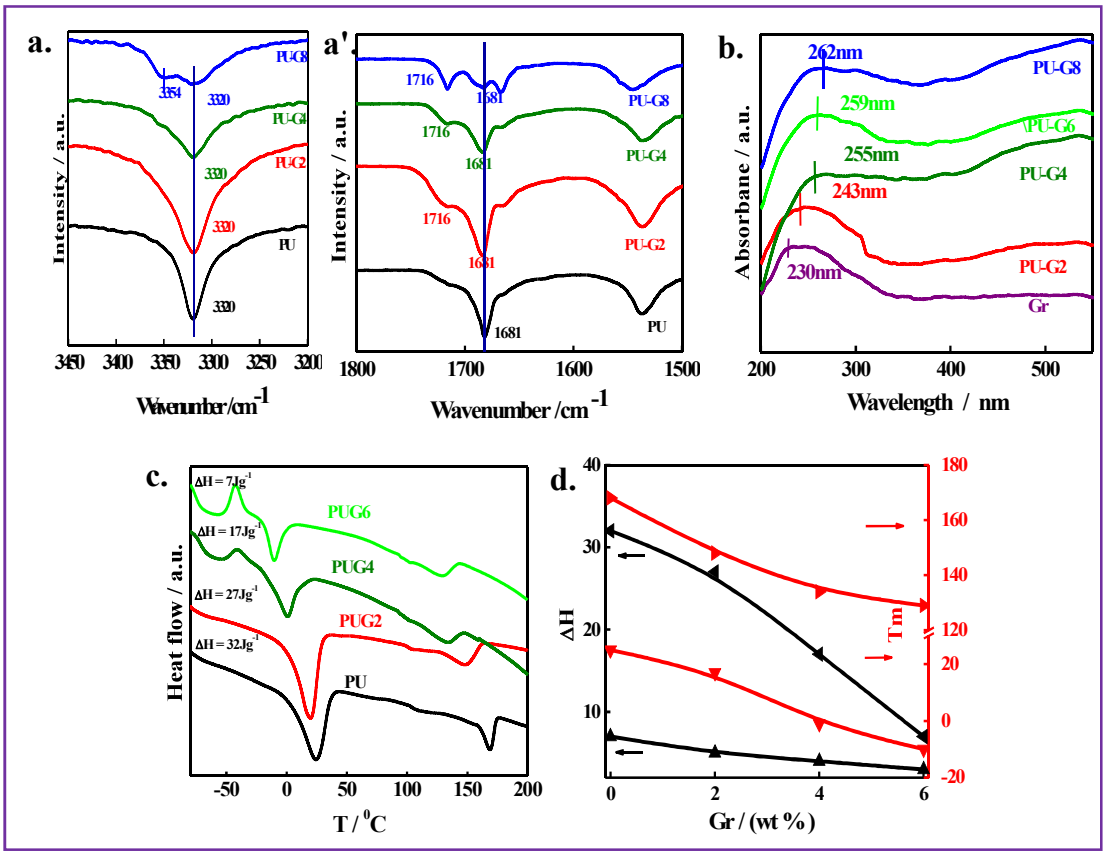

Figure 3.4: (a, a') FTIR spectra of PU and its indicated nanocomposites showing peak position shifted in nanocomposites as compared to pure PU; **(b)** UV-visible spectra of PU and its indicated nanocomposites exhibiting absorption peaks; **(c)** DSC thermograms of PU and its indicated nanocomposites showing heat of fusion; **(d)** Plot of heat of fusion and melting temperature vs. percentage graphene content.

Effect of graphene on crystallinity in PU nanocomposites has also been studied through XRD measurements showing considerable reduction of intensity of the peak at 23.6^0 for nanocomposites as compared to strong peak observed for pure PU (Figure 3.5), supporting the DSC studies of lower heat of fusion for higher graphene content nanocomposites. In higher graphene content PU-G8 less crystalline nature is evident from XRD pattern and its prominent exothermic peak in DSC clearly indicates the cold crystallization followed by its melting and the intensity of the cold crystallization peak

increase with graphene content signifying the nucleating nature of graphene. Decrease in heat of fusion for soft segments has also reported by Nguyen et al. (2009) but there was no alteration of T_m, of PU matrix in presence of graphene [Nguyen et al. (2009)]. Suppression in heat of fusion and T_m of PU in presence of organically modified nanoclay has also reported by Mishra et al. [Mishra et al. (2010)]. Nguyen et al. (2009) has been used the aromatic based diisocyanate (MDI) which are unable to form self-assembled structure through the hydrogen bonding interaction whereas, in our case HMDI was used and thereby the urethane linkages are able to form strong hydrogen in the hard segment. Thus, strong interaction between graphene and PU in this work is justified where both soft and hard segment interact with graphene as explained in the literature as well. However, the strong interaction between graphene and PU is established through FTIR, UV-vis and DSC studies clearly indicating two different types of interactions in pure PU (hydrogen bonded) and PU-graphene nanocomposites (predominantly dipolar interactions).

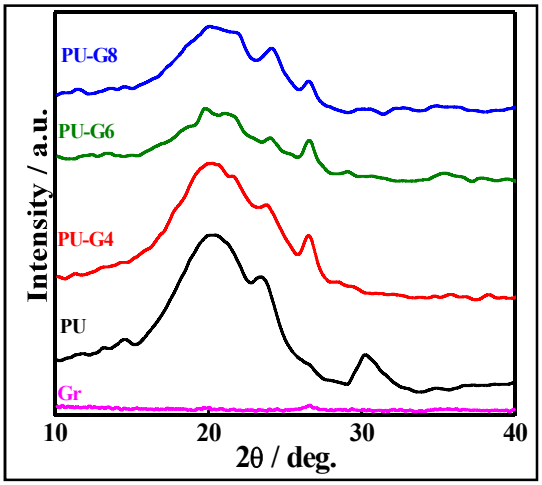

Figure 3.5: Wide-angle X-ray diffraction of PU and its indicated nanocomposites, showing the reduced in the intensity of polymer nanocomposites as compared to pure PU and the intensity further reduced when the content of graphene is increased.

3.2.3 Mechanical behavior:

Mechanical behavior of pure PU and its different nanocomposites under uniaxial stress (stress-strain curve) through universal tensile machine have been shown in (Figure 3.6a). The nanocomposites show lower tensile modulus (calculated from the initial linear region) as compared to pure PU while the elongation at break is greater for nanocomposites exhibiting higher toughness (measured from the area under stress-strain curve) as compared to pure PU. (Figure 3.6b) represents the relative values of modulus and toughness of pure PU and its nanocomposites. Decrease in modulus value of nanocomposites is explained from the significant lowering of crystallinity of PU in presence of graphene as observed in DSC and XRD studies. Moreover, the stress transfer mechanism gets facilitated in nanocomposites [Liang et al. (2009)], because of significant interactions in exfoliated system and more amorphous contribution, as discussed above, causing higher toughness of nanocomposites as compared to pure PU. It has been observed that toughness is increased up to 6 wt.% of graphene in nanocomposites followed by its sharp decrease is mainly due to agglomeration of graphene at higher concentration leading to catastrophic failure.

In liquid state, mechanical strength of pure PU and its nanocomposites was determined by rheological experiment at 210^0C (T_m (PU) + 40^0C) over a wide range of angular frequency (ω). Significant enhancement in the storage modulus G/(ω) for nanocomposites was observed as compared to pure PU throughout the whole frequency range indicating greater melt strength of nanocomposites in presence of graphene (Figure 3.6c). However, the melting temperature of nanocomposites are much lower as compared to pure PU (from DSC curves; Figure 3.4c) and therefore it is expected to

show lesser mechanical strength at 210^0C (T_m + 75^0C for PU-G4) but, a strong networking in presence of graphene along with strong interaction with the filler transform the nanocomposites into greater melt strength. Therefore, strong network structure, due to the self-assembly process, form stacks which certainly has an effect on mechanical behavior in liquid state. On the other hand, a dip point is observed in storage modulus curves at 60 rad s^{-1} for pure PU whose positions get shifted gradually towards higher frequency for increased graphene content nanocomposites presumably due to the splintering of the network structure occurs at that frequency region, depending on the strength of nanostructure, and higher dip frequency for nanocomposites appears due to greater strength of the stacks in nanocomposites arising from greater interaction between graphene and PU matrix. Increase in the depth of dip was observed with increasing graphene content in nanocomposites. This is due to initial higher strength of stacks in nanocomposites in presence of more graphene which get splintered giving rise to greater dip in higher graphene content nanocomposites. Furthermore, increase in storage modulus after the dip is due to the reformation/rearrangement of network structure at higher frequency. The complex viscosities of PU and its nanocomposites exhibits the similar behavior like storage modulus and initially it decreases and reach a minima with increasing frequency indicating the breakage of structure occurred at a particular frequency followed by its increasing tendency due to the reorganization of the structure at higher frequency (Figure 3.6d). Rheological experiment clearly indicates the greater and stronger networking structure in two representative nanocomposites as compared to pure PU due to the greater interaction between polymer matrix and graphene layers.

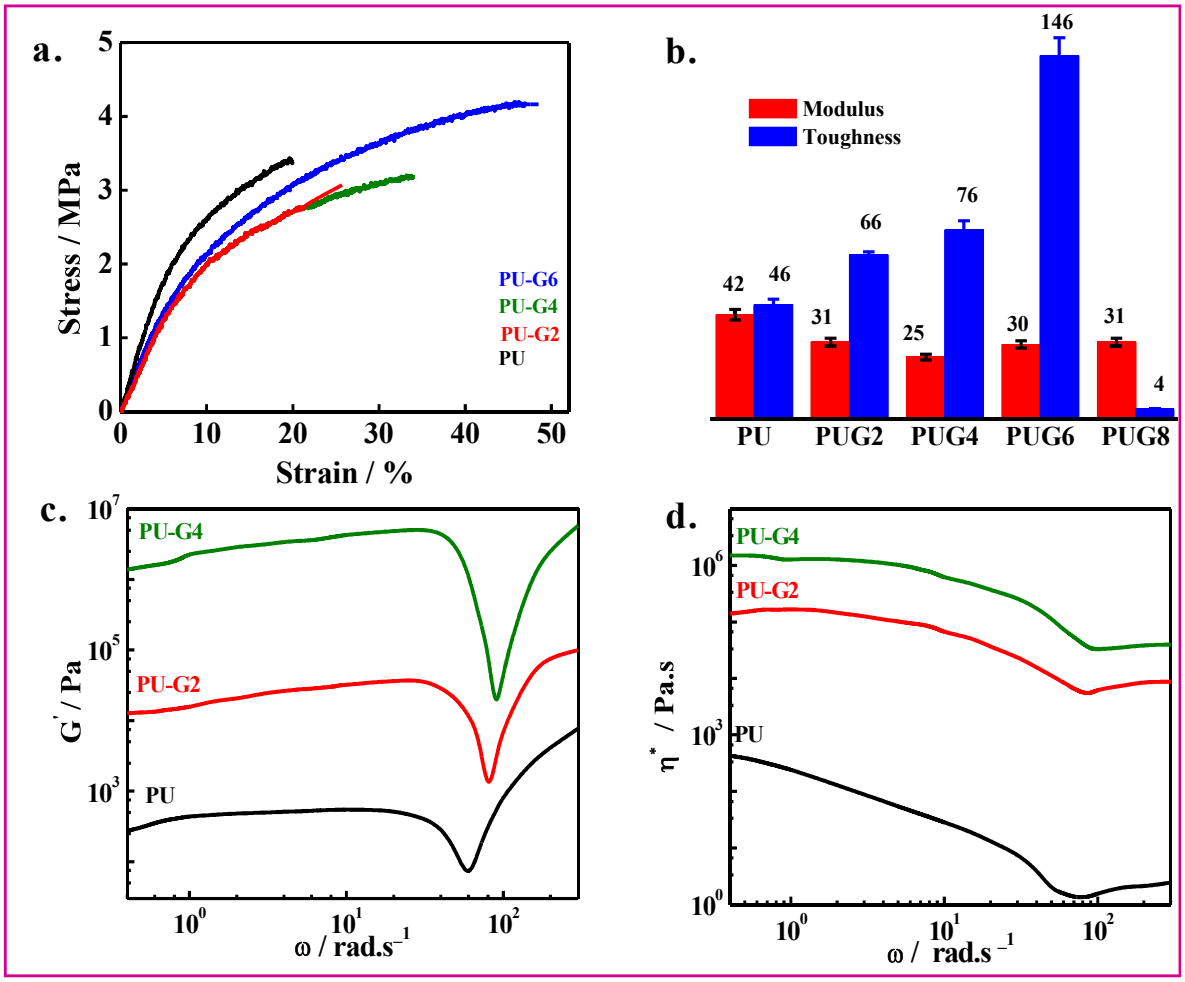

Figure 3.6: Mechanical properties of PU and its indicated nanocomposites in solid and liquid State **(a)** Stress-strain curves of pure PU and its nanocomposites; **(b)** Comparison of modulus (MPa) and toughness (MJm^{-3}) values of PU and its nanocomposites as indicated in the bar graph; **(c)** storage modulus and **(d)** complex viscosity of pure PU and its nanocomposites as a function of frequency.

Moreover, the storage modulus increases by two orders of magnitude (4×10^8 Pa for PU-G4) upon decreasing the temperature by 20^0C ($210 \rightarrow 190^0$C) from its value of 4×10^6 Pa for PU-G4 at 210^0C. Storage modulus and complex viscosity of pure polyurethane and its nanocomposites at 190^0C has been given in (Figure 3.7).

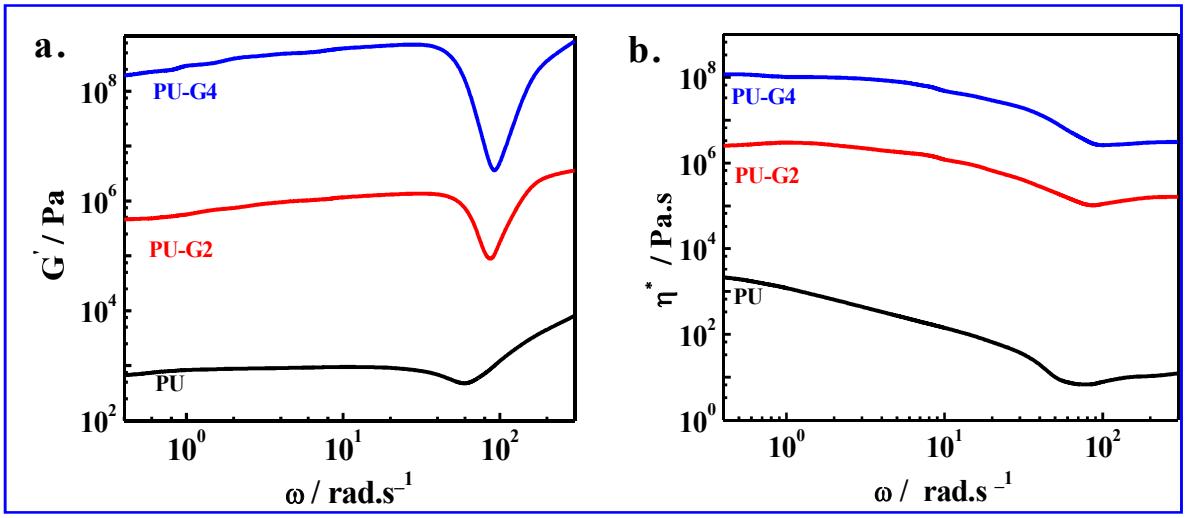

Figure 3.7: Melt state mechanical behavior of pure PU and its indicated nanocomposites. **(a)** Storage modulus and **(b)** complex viscosity of pure PU and its indicated nanocomposites as a function of Frequency at 190^0C, showing the enhancement in melt state mechanical property of nanocomposites as compared to pure PU.

3.2.4 Thermal properties:

The thermal behavior of pure PU and its nanocomposites has been studied through thermogravimetric analyzer (TGA) and TGA thermograms are shown in (Figure 3.8). Pure PU exhibits the double degradation pattern due to different degradation process of hard segment, degrade at lower temperature and soft segment zone, and degrade at higher temperature, reflecting their relative abundance in overall PU chains [Rogulska et al. (2007)]. Decrease in the degradation temperature of nanocomposites has been observed with increasing graphene content indicating lesser thermal stability of nanocomposites. Closer look of the patterns indicate that the degradation temperature of soft segment of nanocomposites remain unaltered at 400^0C while the hard segments

of nanocomposites start degrading at lower temperature arising from its smaller size, larger in number and uniform distribution of hard segmented stacks in nanocomposites as compared to pure PU. Similar kinds of degradation behavior of PU in presence of modified graphene has been reported by Nguyen et al. [Nguyen et al. (2009)]. Furthermore, enhancement in the thermal stability of PU has been reported in presence of inorganic nanoclay [Gilman et al. (2000)] while better thermally conducting graphene decrease the thermal stability of PU.

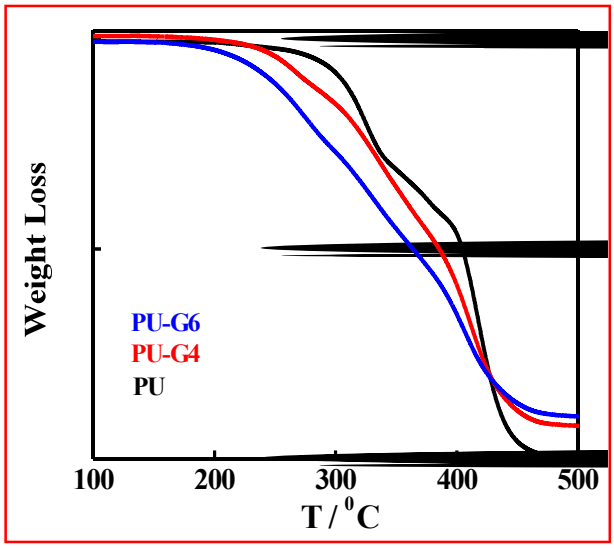

Figure 3.8: Degradation behavior of PU and its indicated nanocomposites in nitrogen atmosphere.

3.2.5 Enzymatic degradation:

Being used as biomaterial, it is important to study the biodegradation behavior of PU in enzyme medium and how it gets modified in presence of grapheme. (Figure 3.9a and b) shows the biodegradation in two different enzymes *(lipase and protease)* comparing PU and its nanocomposites showing significantly higher biodegradation rate of nanocomposites than that of PU. Nearly 55 and 65% weight losses occurs in

protease and lipase medium against the 17 and 30% biodegradation for pure PU in respective enzyme indicating slightly better efficacy of lipase enzyme over the protease towards the biodegradation of PU. The relative higher rate of enzymatic degradation in nanocomposites is due to the lower crystallinity, as supported through XRD and DSC measurements, as compared to the pure PU. It is noteworthy to mention that biodegradation takes place through hydrolytic mechanism and amorphous zone is more prone to hydrolysis [Maiti et al. (2007)]. Even though graphene is considered to be non-biodegradable, higher biodegradation rate of other polymers in presence of graphene have been reported while there is no literature reported data for PU [Sridhar et al. (2013); Li et al. (2012)]. The cause of greater biodegradation of PU in presence of graphene may lie on the two dimensional solid support of graphene which might act as better catalytic system [Singh et al. (2013)]. However, the biodegradation can be enhanced by using graphene as the filler and the rate can be regulated by altering the content of graphene in nanocomposites.

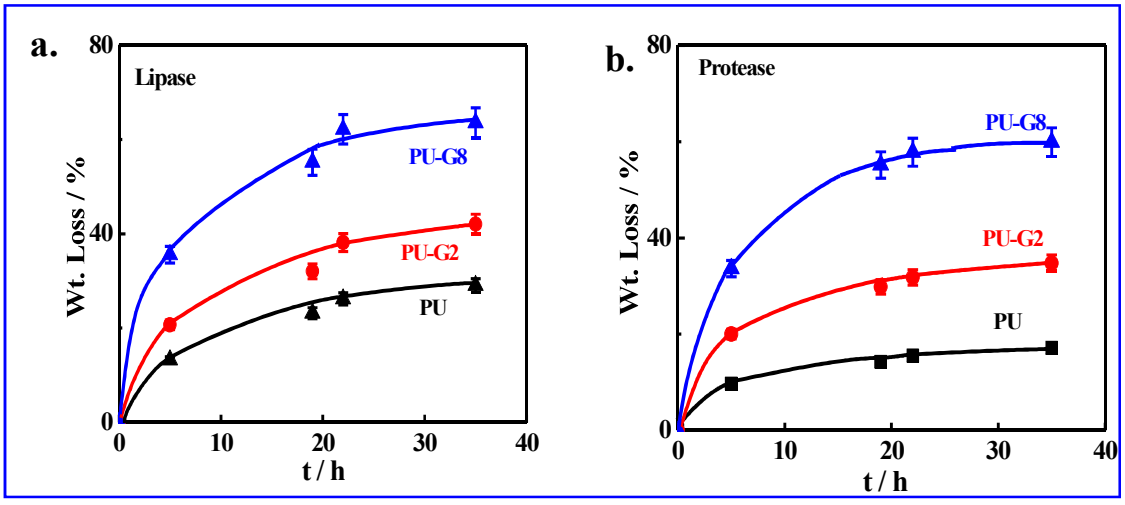

Figure 3.9: Enzymatic degradation of pure PU and its indicated nanocomposite; (a) through *lipase* and (b) *protease*

3.2.6 Drug release:

In-vitro drug release of the antibiotic (Tetracycline hydrochloride) loaded drug from the pure PU and its nanocomposites in phosphate buffer solution (pH~7.4) at 37^0C have been done through UV-visible absorption technique [Schierholz et al. (1997); Kwok et al. (1999)]. It is necessary for materials to use as implant is that the polymer unlike metals can release the biologically active materials at a suitable rate as per the requirement of the biological environment for a desire time period [Singh et al. (2012)]. Standard curve was drawn after taking absorbance using 360 nm in concentration range of 1-100 μg/ml and concentration of release drug was measured through UV-visible absorbance. Standard curve of drug is given in (Figure 3.10).

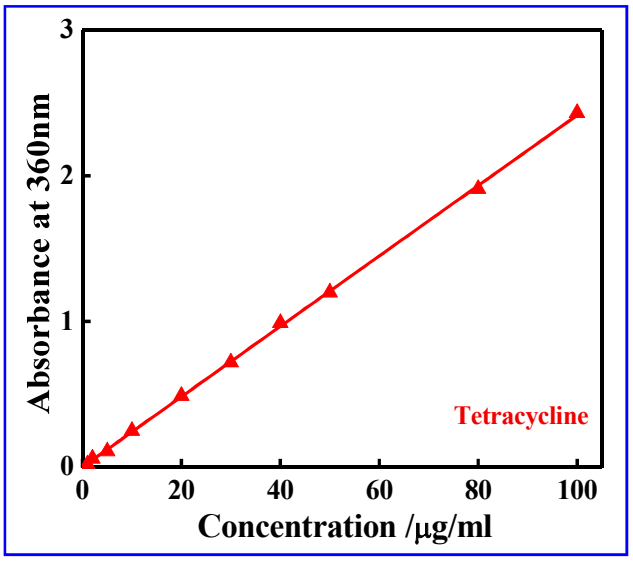

Figure 3.10: Standard curve of Tetracycline Hydrochloride standard stock solution (1mg/ml) drawn after taking absorbance using UV-visible spectrometer at 360 nm in the concentration range of 1-100 μg/ml.

(Figure 3.11a) shows the cumulative percentage release as a function of time and it was observed that burst release of ~35 wt. % of loaded drug in pure PU followed by its

gradual release up to 60 wt. % in 10 days. However, in case of nanocomposites sustained release of drug has been observed without any burst release and overall suppressed but steady release is noticed with increasing graphene content in nanocomposites. Interaction between the components and diffusion kinetics in the medium is the major factor which affects the release of drug either from pure polymer or its nanocomposites. The release kinetics of drug from pure PU and its nanocomposites were best fitted with the Korsmeyer-Peppas model ($r^2 \sim 0.996$) and given in (Figure 3.11b) leading to the exponent *'n'* values of 0.53, 0.57, 0.64 and 0.68 for PU, PU-G2, PU-G4 and PU-G8, respectively (Table 3.1). The higher values of exponent in nanocomposites indicate a delayed diffusion due to the presence of two-dimensional graphene sheet in polymer matrix which creates the "tortuous path". On the basis of drug release kinetics, a model has been proposed where in pure PU diffusion of drug molecules is relatively easy in presence of hard segmented cluster being the only barrier against the two dimensional graphene layers along with distributed hard segmented zone clearly make a lot of hindrance to pass through a tortuous path in nanocomposites causing delay in delivery (Figure 3.11c). For release of the loaded drug from polymer matrix few steps involved and these are liquid penetration into the matrix, dissolution of the drug and their diffusion phenomena, and out of these steps, any one may be responsible for the rate determining step of drug release [Depan et al. (2009)]. Nanocomposites exhibit the slow release as compared to pure PU and release rate is decreased drastically with increasing the content of graphene and this decrease is presumably due to the barrier effect of the two-

dimensional graphene by which the drug molecule gets hindered causing sustained release in nanocomposites.

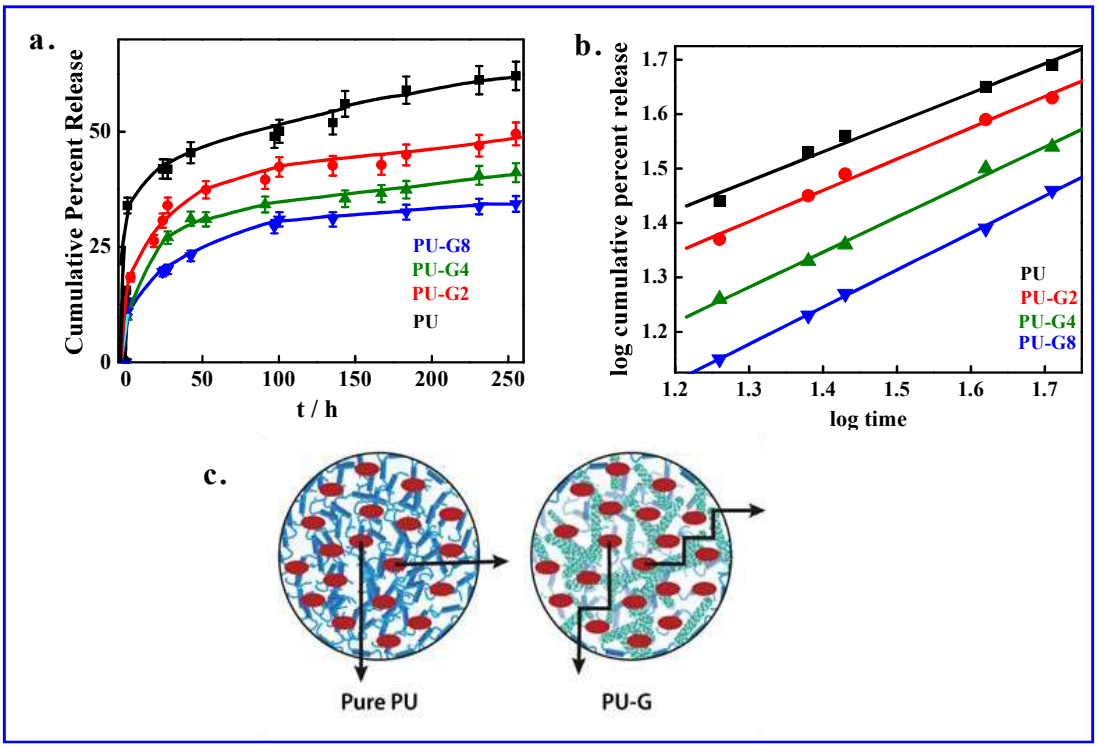

Figure 3.11: (a) Sustained drug release profile of pure PU and indicated nanocomposites; **(b)** Korsmeyer-Peppas fitting in pure PU and its indicated nanocomposites **(c)** Schematic model of drug release kinetics. The red sphere and green plates indicates the drug and graphene sheet, respectively. The arrows indicate the probable path of drug diffusion in pure PU and nanocomposites demonstrating sustained delivery in nanocomposites as compared to pure PU.

Sample	Zero Order		First Order		Higuchi		Korsmeyer-Peppas	
	k	r^2	k	r^2	k	r^2	n	r^2
PU	0.49 ± 0.02	0.991	1.12 ± 0.02	0.992	5.71 ± 0.28	0.996	0.53 ± 0.03	0.992
PU-G2	0.48± 0.03	0.993	1.10 ± 0.03	0.993	5.61 ± 0.21	0.997	0.57 ± 0.02	0.996
PU-G4	0.44 ± 0.03	0.990	1.01 ± 0.03	0.990	5.17 ± 0.28	0.995	0.64 ± 0.02	0.997
PU-G8	0.42 ± 0.02	0.995	0.96 ± 0.02	0.995	4.82 ± 0.40	0.989	0.68 ± 0.01	0.999

Table 3.1: Release rate constant (k), correlation coefficient (r^2) and diffusion release exponent (n) obtained using different mathematical models for drug loaded PU and its indicated nanocomposites.

3.2.7 Cell Viability and Fluorescence:

For biological application material should be in biocompatible nature and biocompatible nature of pure PU and its nanocomposites was monitored on bone marrow derived mesenchymal stem cells (BMMSCs) in term of cell viability, fluorescence and cell adhesion. Cell viability of the bone marrow derived mesenchymal stem cells (BMMSCs) on pure PU and its nanocomposites has been studied through MTT assay at different time intervals and has been shown in (Figure 3.12a). Viability of cells seeded on culture medium without any specimen was taken as a control. After one day time interval the cell viability of pure PU and its nanocomposites was found to be ~ 40% after 1 day which has further increased to ~70% after 5 days indicating biocompatible nature of PU and its nanocomposites [Zhu et al. (2011)]. No adverse effect of graphene at high concentration was observed on cell growth which had also been reported in the literature using stem cells [Nayak et al. (2011)]. Surface chemistry such as hydrophobic / hydrophilic nature, wettability and topographical parameter like roughness, texture plays an important role in cell proliferation process because of initial attachment implying the physicochemical connections between surface and cells through ionic forces [Leenaerts et al. (2009)]. Fluorescence image of cell proliferation studies also support the MTT assay clearly indicating more number of cells grown on nanocomposites as compared to pure PU and control (Figure 3.12b). The number density of cell of control, PU, PU-G2 and PU-G6 are 6, 11, 16 and 19 per square centimeter, respectively, suggesting PU as biomaterial and nanocomposites are classified as better biocompatible than that of PU.

3.2.8 Cell adhesion:

Cell adhesion parameter tells about the possible nature of material to use as implant one. Biocompatibility of PU and its nanocomposites have been evaluated in vitro in terms of cell adhesion and cell proliferation by using the bone marrow derived mesenchymal stem cell (BMMSCs). The bar diagram of cell adhesion on PU and its nano composites are shown in (Figure 3.12c). The optical density of the cells seeded in the medium without any specimen was taken as a control. The optical density was 2.30, 3.00, 4.36, 4.15, 4.29, and 4.18 in the control, pure PU, PU-G2, PU-G4, PU-G6 and PU-G8, respectively. Higher optical density of nanocomposites (measure of cell adhesion) as compared to the control and pure polymer clearly indicating higher cell adhesion on the nanocomposites resulting from better biocompatibility of the nanocomposites vis-à-vis pure polymer. It has been also reported that the pure graphene film exhibits biocompatible nature through cellular adhesion using human mesenchymal stem cells [Kalbacova et al. (2010)] and it is expected that the cell adhesion may increase even when it is wrapped with another biocompatible polymer like polyurethane.

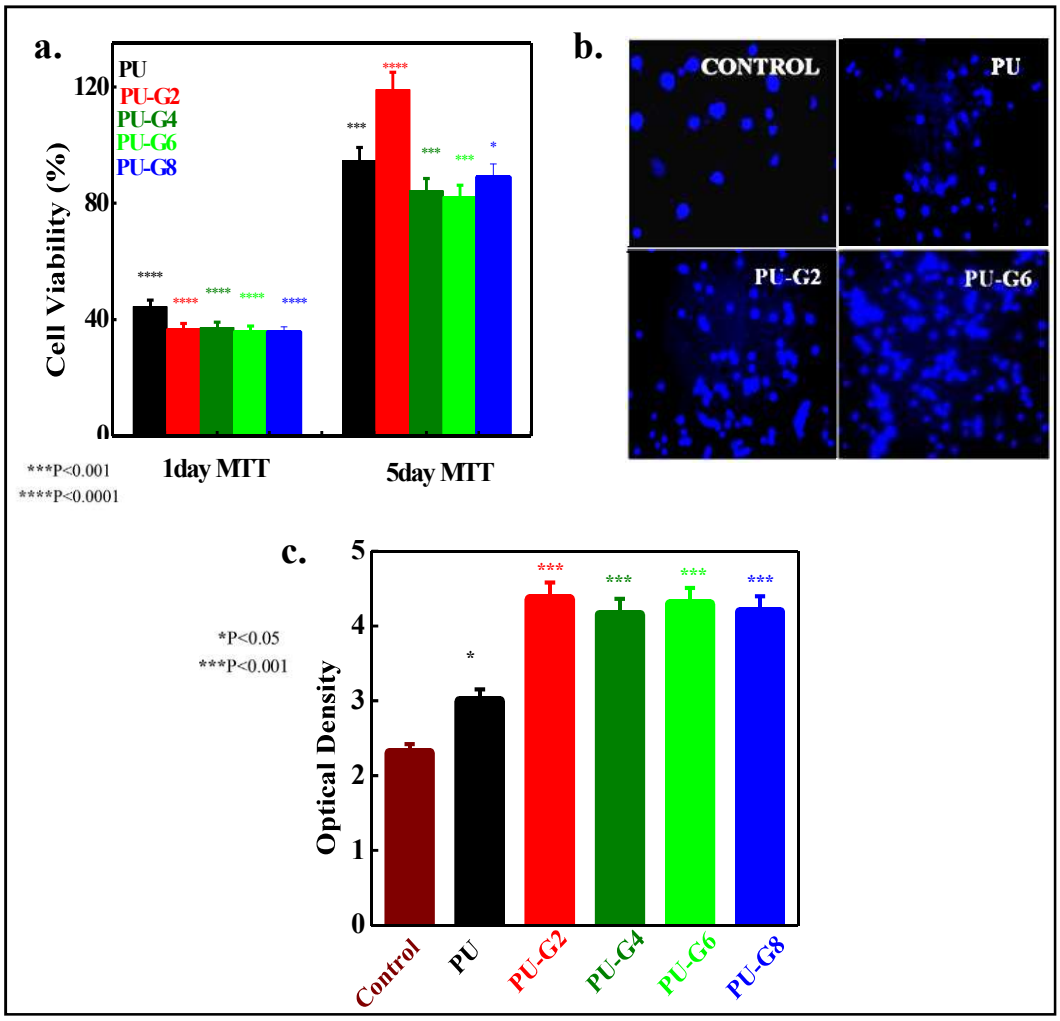

Figure 3.12: Biological studies on pure PU and its indicated nanocomposites. **(a)** BMMSCs cell viability of pure PU and its nanocomposites with time interval of 1 and 5 days; **(b)** Fluorescence microscopic image of cell cultured on PU and its indicated nanocomposites after 1 day of cell proliferation; **(c)** BMMSCs cell adhesion on PU and its indicated nanocomposites in terms of optical density. The absorption value was taken at 570 nm.

3.3 Conclusion:

Different nanocomposites of polyurethane have been synthesized by dispersing graphene sheets in the early stage of polymerization (*in situ*) followed by its chain extension ensuring the best dispersion, revealed through bright filed TEM image. Effect of graphene on layer by layer self-assembly has been demonstrated starting from nanometer scale (XRD and SANS measurements) to micron scale (optical images) via submicron scale through AFM. The strong interactions between polyurethane and graphene have been shown through FTIR and UV-vis spectroscopy from considerable shifting of peak positions. DSC measurement indicates the depression of melting point and decrease of heat of fusion of both the hard and soft segments with increasing graphene content strongly suggest good interactions with graphene and the whole polymer chain (soft and hard segments). Stress strain curves show considerable improvement in toughness in nanocomposites while a trade-off has been observed for stiffness because of amorphization in nanocomposites due to increased interactions. Nanocomposites exhibit the higher storage modulus in the melt state due to self-assembly while splintering of cluster occurs at a particular frequency, depending on the strength of cluster; more for higher graphene content nanocomposites, followed by their reformation at higher frequency, as appeared from a dip in storage modulus vs. frequency measurement. Nanocomposites show the faster biodegradation as compared to pure polyurethane. Controlled and sustained release of tetracycline hydrochlorids an antibiotics loaded drugs has been observed in nanocomposites rendering delayed diffusion in nanocomposites in presence of two-dimensional graphene sheet and small distributed clusters against burst release noticed in pure polyurethane. Biocompatibility

natures of nanocomposites were verified through MTT assay, cell proliferation and cell adhesion measurement.